Organic & Biomolecular Chemistry

A β-Hairpin Peptide Derived from Aβ Forms Different Oligomers in the Crystal State and in Aqueous Solution

Journal:	*Organic & Biomolecular Chemistry*
Manuscript ID	OB-ART-02-2025-000296
Article Type:	Paper
Date Submitted by the Author:	17-Feb-2025
Complete List of Authors:	Zhu, Jason; University of California Irvine Kreutzer, Adam; University of California Irvine Liu, Zhiwei; Rowan University Li, Xingyue; University of California Irvine Richter, Sabrina; University of California Irvine Pophristic, Vojislava; Rowan University Nowick, James; University of California Irvine

ARTICLE

A β-Hairpin Peptide Derived from Aβ Forms Different Oligomers in the Crystal State and in Aqueous Solution

Received 00th January 20xx,
Accepted 00th January 20xx

DOI: 10.1039/x0xx00000x

Jason Zhu,[a] Adam G. Kreutzer,[a] Zhiwei Liu,[b] Xingyue Li,[a] Sabrina M. Richter,[a] Vojislava Pophristic,[b] and James S. Nowick*[a,c,d]

The supramolecular assembly of amyloid-β into soluble oligomers is critical Alzheimer's disease (AD) progression. Soluble Aβ oligomers have emerged as neurotoxic species involved in AD progression and some Aβ oligomers are thought to be composed of β-hairpins. In this work, we report the X-ray crystallographic and solution-phase assembly of a macrocyclic β-hairpin peptide that mimics a β-hairpin formed by $Aβ_{16–36}$. In the crystal lattice, the peptide assembles into a symmetric hexamer composed of two identical triangular trimers. In aqueous solution, the peptide assembles to form an asymmetric hexamer. ^{1}H NMR, TOCSY, and ^{1}H,^{15}N HSQC experiments establish that the asymmetric hexamer contains two different species, **A** and **B**. ^{15}N-edited NOESY reveals that species **A** is a cylindrin-like trimer and species **B** is a triangular trimer that collectively constitute the asymmetric hexamer. Diffusion-ordered NMR spectroscopy (DOSY) suggests that two asymmetric hexamers further assemble to form a dodecamer. NMR-guided molecular mechanics and molecular dynamics studies provide a model for the asymmetric hexamer and suggest how two asymmetric hexamers can form a dodecamer. Solution-phase NMR studies of analogues show that intermolecular hydrogen bonding and the formation of a hydrophobic core help stabilize the asymmetric hexamer. These NMR and crystallographic studies illustrate how an Aβ β-hairpin peptide can assemble to form different well-defined oligomers in the crystal state and in aqueous solution, providing a deeper understanding of the heterogeneity of Aβ oligomers and new structural models of Aβ oligomers composed of Aβ β-hairpins.

[a] *Department of Chemistry, University of California, Irvine, Irvine California 92697-2025, USA.*
[b] *Department of Chemistry and Biochemistry, Rowan University, Glassboro, New Jersey 08028-1701, USA.*
[c] *Department of Pharmaceutical Sciences, University of California, Irvine, Irvine California 92697-2025, USA.*
[d] *Department of Molecular Biology and Biochemistry, University of California, Irvine, Irvine California 92697-2025, USA.*

† Electronic Supplementary Information (ESI) available. See DOI: 10.1039/x0xx00000x

Introduction

Supramolecular assembly of amyloid-β (Aβ) peptide into soluble toxic oligomers and insoluble fibrils is central to Alzheimer's disease (AD) pathogenesis.[1–3] While advances in cryogenic electron microscopy and solid-state NMR spectroscopy have provided structural insights into different Aβ fibril polymorphs, the structures of soluble Aβ oligomers remain largely unknown.[4–9] The metastability and heterogeneity of soluble oligomers have hampered structural elucidation by high-resolution techniques such as X-ray crystallography and solution-phase NMR spectroscopy.

β-Hairpins have emerged as building blocks of many soluble Aβ oligomers. The β-hairpin conformation was originally postulated by Pollard and coworkers in 1994 and supported by subsequent *in silico* models.[10–12] In 2008, Härd and coworkers reported the first high-resolution NMR structure of $Aβ_{1–40}$ in a β-hairpin conformation and postulated that the β-hairpin conformation is involved in the formation of oligomers.[13] In a subsequent study, Härd and coworkers constrained $Aβ_{1–40}$ and $Aβ_{1–42}$ into β-hairpin conformations through intramolecular disulfide linkages and found that disulfide-stabilized Aβ β-hairpins exhibited greater propensity to oligomerize than the unconstrained Aβ peptides.[14] Yu and coworkers have also demonstrated that $Aβ_{1–42}$ can assemble to form soluble oligomers composed of Aβ β-hairpins.[15] Additional work by Okumara and coworkers clarified the role of Arg_5 in the formation of β-hairpins for $Aβ_{1–40}$ and $Aβ_{1–42}$.[16] The multiple possible β-hairpin registrations reflects the polymorphic nature of soluble Aβ oligomers. It is still unclear which β-hairpin registration is the predominant assembly formed by full-length Aβ oligomers. Collectively, these early *in silico* and experimental studies support the importance of the β-hairpin conformation in soluble Aβ oligomers.

More recently, seminal work by Carulla and coworkers elucidated the first high-resolution solution-phase NMR structure of a soluble Aβ oligomer.[17] This $Aβ_{1–42}$ tetramer contains a six stranded β-sheet formed by two β-hairpins and two antiparallel β-strands. Size exclusion chromatography and native ion mobility mass spectrometry support the formation of an octamer at higher peptide concentrations consisting of a β-sheet sandwich of two tetramers. Molecular dynamics (MD) simulations suggest how the tetramers and octamers may form pores in cell membranes, leading to cell toxicity. This work underscores how high-resolution structural studies of Aβ oligomers shed light on potential mechanisms of soluble Aβ oligomers toxicity.

Our laboratory has reported the X-ray crystallographic structures of several Aβ oligomer models formed by macrocyclic β-hairpin peptides designed to mimic native Aβ β-hairpins.[18,19] In these β-hairpin peptides, we constrain amyloidogenic fragments from the central and *C*-terminal regions of Aβ into a macrocycle using two δ-linked ornithine turn units.[20] To prevent uncontrolled aggregation, we incorporate an *N*-methyl amino acid that disrupts intermolecular hydrogen bonding. In studying different Aβ β-hairpins peptides, we have observed twisted dimers, triangular trimers, barrel-like tetramers, compact hexamers, ball-shaped dodecamers, and annular pore structures, illustrating the numerous assemblies that Aβ β-hairpin peptides can form.[18,19] Several of the Aβ β-hairpin peptides that assemble crystallographically have also been demonstrated to exhibit neurotoxicity and/or have been recognized by A11, an antibody that recognizes Aβ oligomers.[18,21,22]

While X-ray crystallography provides insights into the structures of oligomers formed by β-hairpin peptides in the crystal lattice, this technique only provides a static snapshot of the oligomer structure. Crystal lattice formation typically favors a single, homogenous low-energy structure, that may not reflect the variety of oligomer structures present in solution. Solution-phase NMR spectroscopy thus complements X-ray crystallography with insights into the structures and dynamics of oligomers in aqueous solution.

Here, we set out to characterize the assembly of Aβ β-hairpin peptide **1** using solution-phase NMR spectroscopy.[18] Peptide **1** contains $Aβ_{16–22}$ and $Aβ_{30–36}$ constrained into a macrocycle by two δ-linked ornithine turn units (^{δ}Orn) and an *N*-methyl group on Phe_{19} (Figure **1A**). This particular alignment between the $Aβ_{16–22}$ and $Aβ_{30–36}$ fragments has been proposed Tycko and co-workers based on cryogenic electron microscopy and solid-state NMR spectroscopy data of brain-derived $Aβ_{40}$ fibrils.[6] We previously reported that peptide **1** assembles in the crystal lattice to form a symmetric hexamer composed of two identical triangular trimers (Figure **1B**).[18] In the current study, we found that peptide **1** does not assemble in solution to form a well-defined oligomer that can be fully characterized by solution NMR spectroscopy.

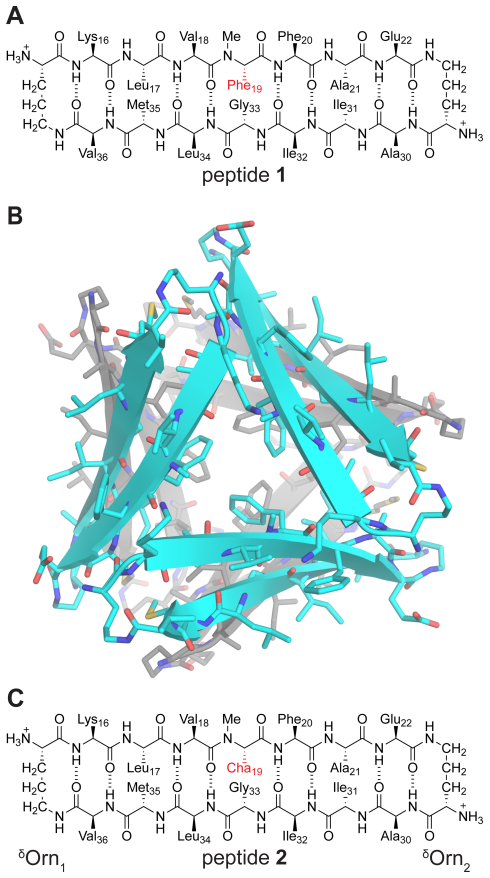

Figure 1. Peptides **1** and **2**, and X-ray crystallographic structure of peptide **1** (PDB 5W4H).[18] Red side chains highlight the Phe-to-Cha mutation. The two triangular trimer subunits of the crystallographic hexamer are colored in cyan and grey.

To promote the solution phase assembly of peptide **1** into a well-defined oligomer, we varied the side chain of Phe_{19} to cyclohexylalanine (Cha) to better pack the hydrophobic core of the crystallographic hexamer. The resulting peptide **2** is shown in Figure **1C**. We hypothesized that solution-phase assembly is driven by hydrophobic core formation, and that Phe-to-Cha mutation would enhance hydrophobic core formation and thus lead to the assembly of a well-defined oligomer. X-ray crystallography shows that peptide **2** assembles to form a symmetric hexamer in the crystal lattice identical to that of peptide **1**, whereby two triangular trimers

assemble in a sandwich-like fashion. Solution-phase NMR spectroscopy reveals that peptide **2** assembles into a well-defined asymmetric hexamer in solution that differs in structure from the symmetric hexamer in the crystal lattice. ^{1}H NMR, TOCSY, and ^{1}H,^{15}N HSQC experiments establish that the asymmetric hexamer is composed of two species, **A** and **B**. ^{15}N-edited NOESY reveals that species **A** is a cylindrin-like trimer and species **B** is a triangular trimer, akin to the trimer observed crystallographically. Species **A** and **B** come together to form a well-defined asymmetric hexamer. Diffusion ordered spectroscopy (DOSY), and MD simulations suggest that two asymmetric hexamers further assemble to form a dodecamer and that the dodecamer is the predominant assembly in solution.

Results and Discussion

Peptide 1 does not assemble to form well-defined oligomers in aqueous solution

In studying the solution-phase assembly of a related class of macrocyclic peptides, our laboratory has established spectroscopic hallmarks indicative of well-defined peptide oligomer assembly in solution.[23,24] These hallmarks include: new resonances appearing as the peptide concentration increases that correspond to an increasing oligomer fraction, downfield shifting of Hα resonances associated with β-sheet structure, upfield shifting of some of the aromatic and methyl side chain resonances associated with hydrophobic packing, a specific reduction in diffusion coefficient associated with the formation of an oligomer of a specific size, and the appearance of new NOE crosspeaks that correspond to intermolecular contacts associated with oligomer formation.

The ^{1}H NMR spectra of peptide **1** lack many hallmarks of oligomer assembly, indicating that peptide **1** does not assemble to form well-defined oligomers (Figure **S1**). At 1.0 mM, the proton resonances of peptide **1** are sharp. At 8.0 and 16.0 mM, the ^{1}H NMR spectra broaden significantly without the appearance of distinct new resonances associated with the formation of a well-defined oligomer. The ^{1}H NMR spectra do not show significant downfield shifting of Hα proton resonances. Although some aromatic and methyl side chain resonances shift upfield slightly, these resonances are broad and not well-defined. The peak broadening in the ^{1}H NMR spectra may reflect exchange between monomer and one or more oligomeric species at an intermediate rate on the NMR timescale.

DOSY is a valuable tool for comparing the relative sizes of oligomers and monomers. When well-defined oligomers assemble in aqueous solution, the diffusion coefficient as measured by DOSY decreases with increasing peptide concentration. The decrease in diffusion coefficient reflects the change in equilibrium from monomer to oligomer. At low peptide concentrations, a single track appears in the DOSY spectrum corresponding to the monomer. At intermediate concentrations, multiple DOSY tracks appear that reflect a change in equilibrium from monomer to oligomer. At high peptide concentrations, a new track appears in the DOSY spectrum corresponding to the oligomer, and the diffusion coefficient of the oligomer remains invariant with further increasing peptide concentration.

DOSY NMR studies reveal that peptide **1** does not form well-defined oligomers of a specific size. At 1.0 mM peptide **1**, the DOSY spectrum shows a monomer with a diffusion coefficient of 1.99 x 10^{-10} m^2/s. At 8.0 mM and 16.0 mM, the DOSY spectra show a single track with a diffusion coefficient of 1.42 x 10^{-10} m^2/s and 0.86 x 10^{-10} m^2/s, respectively. The continuous decrease in the diffusion coefficient with increasing peptide concentration suggests that peptide **1** is in equilibrium with a variety of species of increasing size and the oligomers formed by peptide **1** are not discrete and well-defined.

Peptide 2 assembles to form a hexamer in the crystal state and in SDS-PAGE

The X-ray crystallographic structure of peptide **1** demonstrated that the formation of a hydrophobic core is a key driver of hexamer formation. We hypothesized that mutating Phe_{19}, which contributes to the hydrophobic core of the peptide **1** hexamer, to cyclohexylalanine (Cha) would stabilize the hydrophobic interior of the hexamer and promote the formation of a well-defined oligomer in aqueous solution (Figure **S2**). Studies by Nilsson and coworkers showed how strategic Phe-to-Cha mutations can stabilize fibril formation of $A\beta_{16-22}$ fragments.[25] Our laboratory has also used a Phe-to-Cha mutation to promote the crystallographic assembly of a related macrocyclic peptide.[26] To investigate the effect of the Phe-to-Cha mutation, we compared peptide **2** (the Cha_{19} mutant) to peptide **1** using X-ray crystallography, SDS-PAGE, and circular dichroism (CD) spectroscopy.

Peptide **2** afforded crystals suitable for X-ray diffraction in aqueous HEPES buffer with sodium citrate and isopropanol, nearly identical to the crystallization conditions for peptide **1** (Table **S1**). Elucidation of the X-ray crystallographic structure of peptide **2** reveals that it forms a symmetrical hexamer identical to that of peptide **1**, whereby two triangular trimers pack together in a sandwich-like fashion (Figure **S3**). The amide backbones of the two hexamers overlay with a 0.36 Å RMSD.

The interior of the peptide **2** hexamer is packed with the hydrophobic side chains of Leu_{17}, Cha_{19}, Ala_{21}, Ile_{31}, Gly_{33}, and Met_{35}, while the exterior of the hexamer is decorated by the side chains of Lys_{16}, Val_{18}, Phe_{20}, Glu_{22}, Ala_{30}, Ile_{32}, Leu_{34}, and Val_{36}. A network of 30 intermolecular hydrogen bonds between the six monomer subunits stabilize the crystallographic hexamer (Figure **2**). At the vertices of the triangular trimers, three intermolecular hydrogen bonds stabilize the assembly of the triangular trimers, accounting for 18 hydrogen bonds. At the interface of the two trimers, four intermolecular hydrogen bonds form between adjacent monomers, creating an antiparallel β-sheet, accounting for 12 hydrogen bonds.

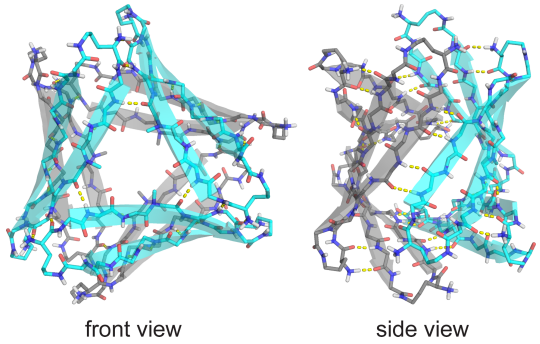

Figure 2. X-ray crystallographic structure of the hexamer formed by peptide **2** (PDB 9EEC). The two triangular trimer subunits of the crystallographic hexamer are colored in cyan and grey. Intermolecular hydrogen bonds are shown in yellow.

To preliminarily evaluate the effect of the Cha mutation on assembly, we used SDS-PAGE, where we ran three different loadings per lane of peptides **1** and **2** (Figure **3**). Peptide **1** migrates as a comet-shaped band near the 10-kDa standard, consistent with the molecular weight of a hexamer (10.6 kDa). The upper bounds of the peptide **1** bands decrease with decreasing peptide

concentration. The concentration dependence and downward streaking of the peptide **1** bands suggest that the hexamer is in equilibrium with lower molecular weight species. Peptide **2** also migrates as hexamers in SDS-PAGE, running as tighter bands that streak less than those of peptide **1**. As the loading of peptide **2** decreases, the upper bounds of the peptide **2** bands decrease less than those of peptide **1**, suggesting the hexamer formed by peptide **2** is more stable than that formed by peptide **1**.

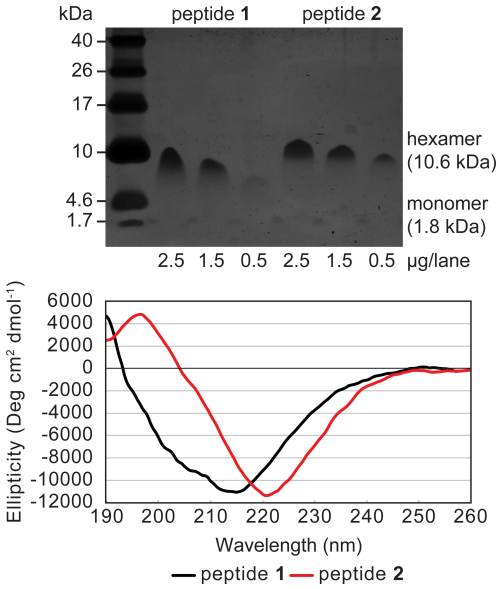

Figure 3. SDS-PAGE and CD spectra of peptides **1** and **2**. SDS-PAGE was performed in Tris buffer (pH 6.8) with 2% (w/v) SDS on a 16% polyacrylamide gel with 2.5, 1.5, and 0.5 µg of peptide per lane and visualized by silver staining. CD spectra were run with 100 µM peptide in 10 mM phosphate buffer at pH 7.4. The contrast of the image of the SDS-PAGE was uniformly adjusted for clarity (Figure **S4**).

We evaluated the secondary structure of peptides **1** and **2** by CD spectroscopy. Peptide **1** shows a strong negative band at ca. 214 nm and a positive band at ca. 190 nm. Peptide **2** displays a strong negative band at ca. 221 nm and a positive band at ca. 196 nm. Although the CD spectra of both peptides show β-sheet structure, peptide **2** appears to reflect a higher degree of folding, as evidenced by the narrower negative band ca. 221 nm and positive band at ca. 196 nm.

X-ray crystallography, SDS-PAGE, and CD spectroscopy studies show that peptide **2** assembles into hexamers in the solid state and in SDS-PAGE, and that it exhibits enhanced β-sheet folding in aqueous solution. Collectively, these studies demonstrate that mutation of Phe_{19} to Cha_{19} does not impact the ability of peptide **2** to form hexamers, and may better stabilize hexamer formation.

Peptide 2 assembles into well-defined oligomers in aqueous solution

The ^{1}H NMR spectra of peptide **2** exhibit many of the hallmarks of well-defined oligomer assembly, such as the appearance of new resonances at higher peptide concentrations associated with oligomer and disappearance of the resonances associated with monomer (Figure **S5**). At 1.0 mM, the ^{1}H NMR spectrum of the peptide **2** monomer is sharp, with notable features including the Cha_{19} Hα proton at 5.68 ppm, aromatic resonances from Phe_{20} at 7.22–7.36 ppm, and methyl resonances from Leu, Ile, and Val at 0.74–1.08 ppm (Figure **4**). At 6.0 mM, oligomeric resonances appear that are roughly equal in intensity to those of the monomer. At 11.0 mM, the oligomeric resonances predominate (Figure **4**).

NH and Hα peak assignments generated through TOCSY and ROESY experiments (further discussed in the subsequent section) reveal that the oligomer appears as two sets of resonances of equal integration, which we term species **A** and **B**. For example, the Cha_{19} Hα proton shows two oligomer peaks at 5.77 and 5.92 ppm increasing in intensity with increasing peptide concentration as the Cha_{19} Hα monomer peak at 5.68 ppm decreases in size and broadens. The peak broadening of the monomer may reflect chemical exchange with the oligomer.[27] Numerous downfield shifted Hα resonances appear for both oligomer species, between 4.91 and 5.92 ppm. Phe_{20} shows one ortho proton resonance for the monomer at 7.25 ppm and two resonances for the oligomer at 7.12 and 7.17 ppm. At 11.0 mM, one of the Leu_{34} methyl resonance appears upfield, at 0.48 ppm, suggesting packing against the Phe_{20} aromatic ring in the oligomer. Thus, the ^{1}H NMR spectra of peptide **2** show many hallmarks associated with the formation of a well-defined oligomer.

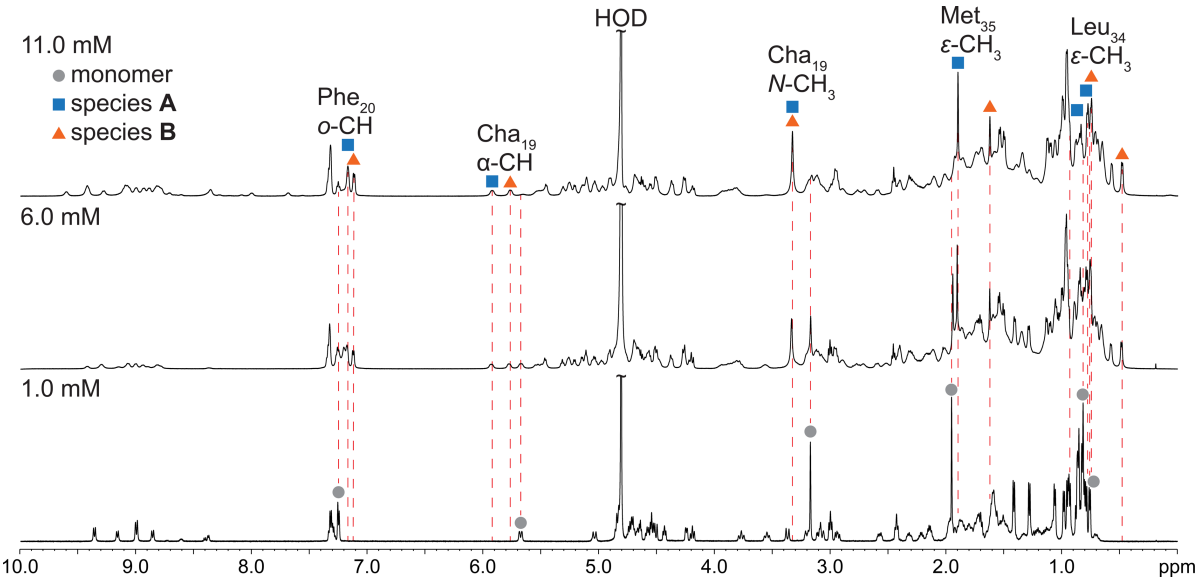

Figure 4. ^{1}H NMR spectra of peptide **2** at 1.0, 6.0, and 11.0 mM in D_2O at 600 MHz and 298 K. Dashed lines highlight key resonances associated with monomer (grey circles), oligomer species **A** (blue squares), and oligomer species **B** (orange triangles). Peaks at 7.5–10 ppm are amide NH resonances that have not fully exchanged with D_2O.

^{1}H,^{15}N HSQC, TOCSY, and ROESY NMR verify the presence of two species, A and B

To corroborate that the oligomer is composed of two distinct species, we introduced an ^{15}N label at Gly_{33} and examined the ^{1}H,^{15}N HSQC spectra of the resulting peptide **2a**. The greater dispersion afforded by the ^{15}N dimension distinguishes each species as a unique crosspeak. At 1.0 mM, the ^{1}H,^{15}N HSQC spectrum of peptide **2a** shows a single crosspeak associated with the monomer at 8.62 ppm in the ^{1}H dimension and 111.4 ppm in the ^{15}N dimension (Figure **5A**). At 11.0 mM, the ^{1}H,^{15}N HSQC spectrum of peptide **2a** shows two crosspeaks at 9.60 and 8.84 ppm in the ^{1}H dimension and 109.9 and 104.7 ppm in the ^{15}N dimension corresponding to species **A** and **B** (Figure **5B** and Table **S2**). The ^{1}H,^{15}N HSQC experiments confirm the peptide **2** oligomer is composed of two spectroscopically distinct species **A** and **B**.

To assign the NH and Hα resonances of the monomer, species **A**, and species **B**, we analyzed the TOCSY and ROESY spectra of peptide **2**. At 1.0 mM, peptide **2** exhibits a single set of resonances associated with the NH and Hα of the monomer in the TOCSY spectrum (Figure **5C**). At 11.0 mM, peptide **2** exhibits two sets of resonances associated with the NH and Hα of species **A** and **B** in the TOCSY spectrum (Figure **5D**). The sequential peak assignments are shown in Figures **S6** and **S7** and are further described in the Materials and Methods section of the Supporting Information.

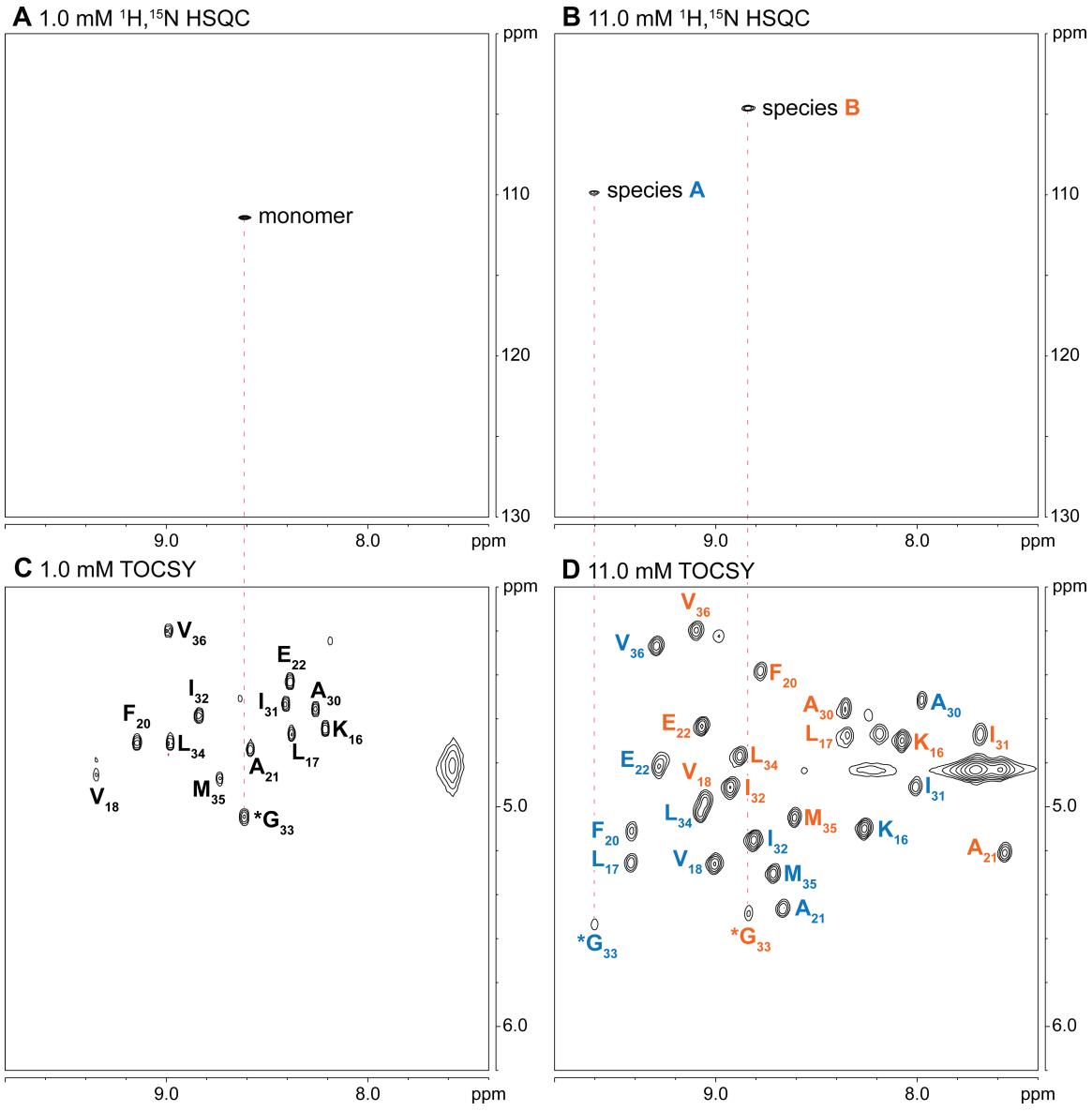

Figure 5. ^{1}H,^{15}N HSQC spectra of peptide **2a** at 1.0 mM (A) and 11.0 mM (B). TOCSY spectra of peptide **2** at 1.0 mM (C) and 11.0 mM (D). Glycine crosspeaks, indicated by an asterisk (*), refer to the *pro-R* Hα. Dashed lines are shown to correlate the glycine crosspeaks of the ^{1}H,^{15}N HSQC and TOCSY spectra. ^{1}H,^{15}N HSQC spectra were recorded at 800 MHz. TOCSY spectra were recorded at 600 MHz. All spectra were recorded in 9:1 H_2O/D_2O at 298 K.

Peptide 2 folds into a β-hairpin conformation in aqueous solution

To investigate the secondary structure and folding of peptide **2** in aqueous solution, we analyzed the chemical shifts of Hα protons, magnetic anisotropy of the diasterotopic $^{\delta}$Orn protons, and intramolecular NOEs associated with β-hairpin formation. The resonances of the peptide **2** Hα protons of the monomer, species **A**, and species **B** are downfield of those that would occur for amino acids in a random coil conformation (Figure **6A** and Table **S3**). This downfield shifting of Hα protons is characteristic of β-sheet secondary structure. The Hα protons of the peptide **2** monomer show an average downfield shift of 0.38 ppm. By comparison, species **A** Hα protons show an average downfield shift of 0.78 ppm and species **B** Hα protons show an average downfield shift of 0.50 ppm. The greater downfield shifting of the oligomer compared to that of the monomer may reflect cooperativity between folding into a β-sheet and oligomerization.

Previous studies have demonstrated that the magnetic anisotropy of the diasterotopic $^{\delta}$Orn protons reflects the extent of folding of the $^{\delta}$Orn turn unit.[20,23,24] In a completely folded macrocyclic β-hairpin peptide, the *pro-S* $^{\delta}$Orn protons appear 0.6–0.7 ppm downfield of the *pro-R* $^{\delta}$Orn protons. In the peptide **2** monomer, $^{\delta}Orn_1$ is well folded, while $^{\delta}Orn_2$ is partially folded (Figure **6B**). In the peptide **2** oligomer, both $^{\delta}$Orn turn units are well folded. The better folding of the turn units further reflects cooperativity between folding into a β-hairpin and oligomerization.

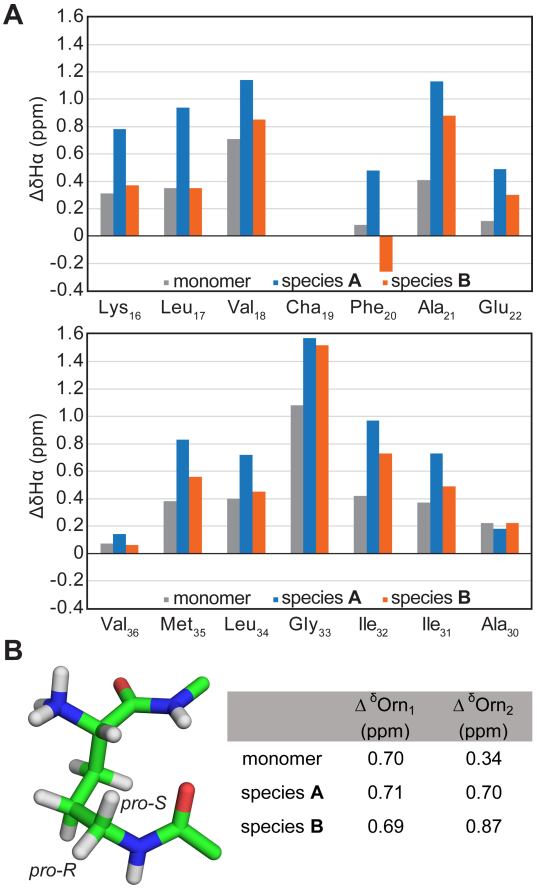

	$\Delta\,^{\delta}Orn_1$ (ppm)	$\Delta\,^{\delta}Orn_2$ (ppm)
monomer	0.70	0.34
species **A**	0.71	0.70
species **B**	0.69	0.87

Figure 6. (A) Chemical shift differences between the peptide **2** Hα protons and random coil values reported by Wishart and Sykes.[28] Cha_{19} was excluded from chemical shift differences analysis because it is a noncanonical amino acid. The chemical shifts of the monomer were recorded at 1.0 mM, and the chemical shifts of the oligomer were recorded at 11.0 mM. (B) Molecular model of the δ-linked ornithine turns unit and magnetic anisotropies of the *pro-R* and *pro-S* protons observed for peptide **2**.

Networks of intramolecular NOEs involving the NH and Hα protons are a spectroscopic hallmark of well-folded β-hairpins. The peptide **2** monomer shows a network of NOEs consistent with β-hairpin folding (Figure **7** and **S8**). When peptide **2** is predominantly oligomeric (11.0 mM), the ^{1}H NMR spectrum is complex, because resonances corresponding to species **A** and **B** are broadened and many are overlapping. Despite the overlap, the NOESY spectra show a network of strong NOEs consistent with well-folded β-hairpins for both species **A** and **B** (Figure **S9**). The NOESY spectra shows interstrand NOEs consistent with all 26 of the expected interstrand contacts associated with folding for both species **A** and **B**. Ten of the 26 NOEs are ambiguous because of heavy spectral overlap.

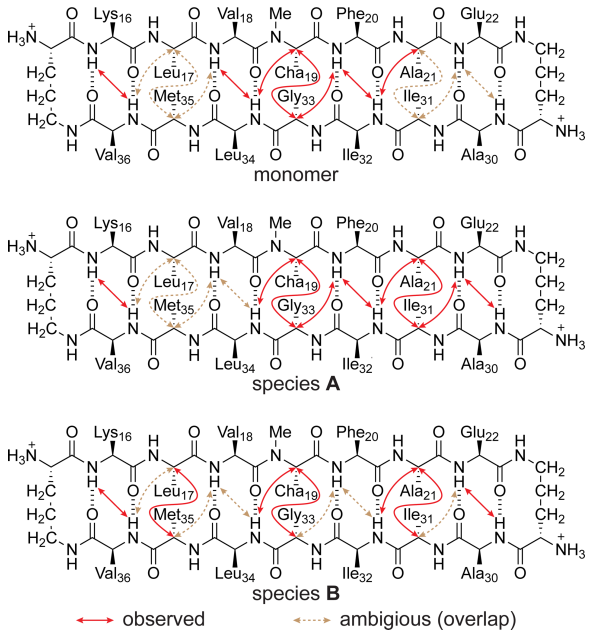

Figure 7. Key intramolecular NOEs for the peptide **2** monomer and oligomer species **A** and **B**. Ambiguous NOEs are indicated by dashed lines. NOEs were identified in the NOESY spectra at 1.0 and 11.0 mM in D_2O and 9:1 H_2O/D_2O at 600 MHz and 298 K.

^{2}H and ^{15}N labeling distinguishes key intermolecular contacts from intramolecular contacts

The NOESY spectra for the peptide **2** oligomer contain many additional NOEs consistent with intermolecular contracts and inconsistent with intramolecular contacts (Figure **S10**). However, many of these intermolecular NOEs are ambiguous due to heavy overlap. To corroborate the assignments of key intermolecular NOEs involving amide NH and Hα protons, we prepared isotopologues **2b–d** that contain selectively incorporated ^{2}H and ^{15}N labels.

To corroborate the assignments of key Hα-to-Hα intermolecular NOEs, we prepared isotopologue **2b**, in which Phe_{20} is deuterated, and isotopologue **2c**, in which both Phe_{20} and Ala_{30} are deuterated. In the NOESY spectrum for the peptide **2** oligomer, we observe strong NOEs between Lys_{16} Hα (species **A**) and Leu_{34} Hα (species **A**), Ala_{30} Hα (species **A**) and Ile_{32} Hα (species **B**), Ala_{30} Hα (species **B**) and Phe_{20} Hα (species **A**), Lys_{16} Hα (species **B**) and Phe_{20} Hα (species **B**) (Figure **8**). When the Hα protons involved in intermolecular contacts are replaced with deuterium, the corresponding NOEs should disappear, and this is what is observed in the NOESY spectra of peptides **2b** and **2c** (Figure **S11**). The disappearance of the NOEs involving the Phe_{20} and Ala_{30} Hα protons supports the assignments of these heavily overlapped NOE crosspeaks.

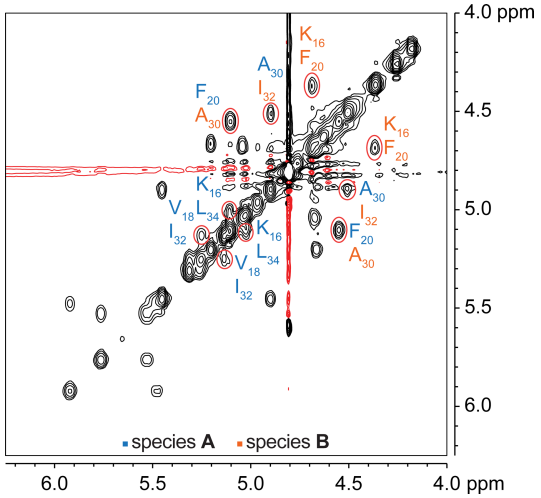

Figure 8. Key Hα-to-Hα intermolecular NOEs in the NOESY spectrum of the peptide **2** oligomer. The spectrum was recorded at 11.0 mM peptide in D_2O at 600 MHz and 298 K.

To corroborate the assignments of key amide NH intermolecular NOEs, we prepared isotopologue **2d**, with ^{15}N labels in the outer facing amide NHs of Leu_{17}, Ala_{21}, Ile_{31}, and Met_{35} (Figure **9A**). ^{1}H,^{15}N NOESY-HSQC spectrum of peptide **2d** was acquired with one increment in the ^{15}N dimension (f_2) and the typical NOESY parameters in the ^{1}H dimensions (f_1 and f_3). The resulting ^{15}N-edited NOESY-HSQC spectrum only shows NOEs involving the ^{15}NH protons. The spectrum exhibits eight distinct vertical tracks, four of which correspond to species **A** and four of which correspond to species **B** (Figure **9B** and **9C**). We assigned the intermolecular NOEs by first assigning the expected intramolecular NOEs and then identifying the remaining intermolecular NOEs — seven ^{15}NH to NH, seven ^{15}NH to Hα, and three ^{15}NH to *N*-Me NOEs. These NOEs support the assignments of the key amide NH intermolecular contacts. A copy of the fully annotated ^{15}N-edited NOESY spectra is shown in Figure **S12**.

Molecular model of the solution-phase asymmetric hexamer

We used PyMOL and MacroModel to construct a constrained NMR-based molecular model consistent with the observed intermolecular contacts and symmetry requirements for the **A** and **B** species (Figure **10**). The **A**-**B** intermolecular contacts in conjugation with the **A**-**A** and **B**-**B** intermolecular contacts indicate one asymmetric oligomer composed of species **A** and **B**, rather than two oligomer species corresponding to species **A** and **B** (Table **1**). The equal integration of the resonances associated with species **A** and **B** suggest that the oligomer contains both species in a 1:1 ratio. The observation of two distinct species in the NMR spectrum rule out the possibility of a symmetric oligomer, such as that observed crystallographically. As we will describe in detail below, the oligomer that best fulfills these requirements and best explains key intermolecular NOEs is an asymmetric hexamer composed of a cylindrin-like trimer (species **A**) and a triangular trimer (species **B**).[29] Additional models that proved inconsistent with the NMR data are further described in Figure **S13**.

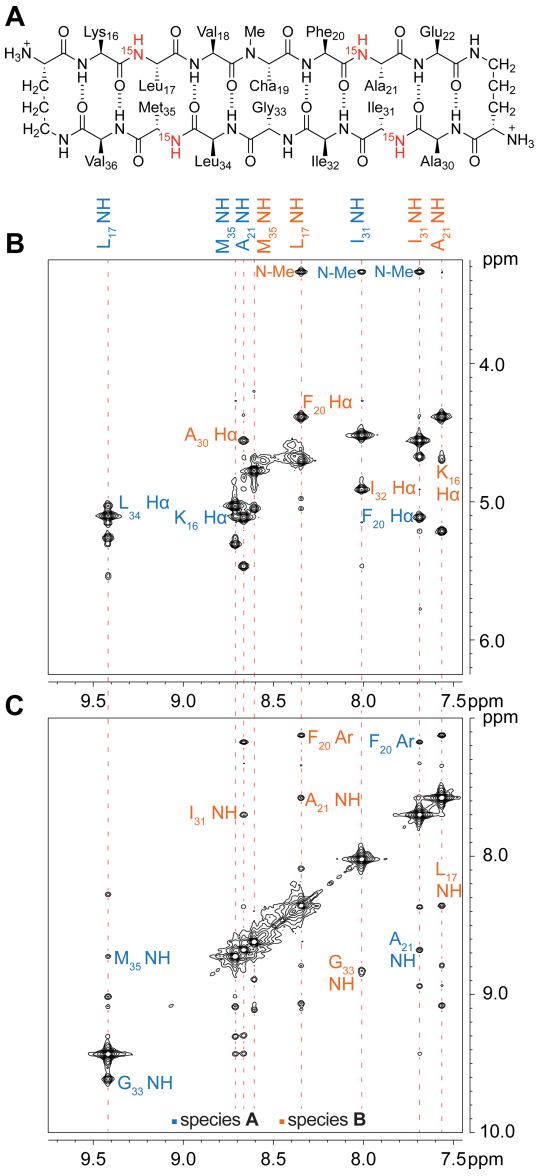

Figure 9. Chemical structure of peptide **2d**, highlighting the ^{15}N labels at Leu_{17}, Ala_{21}, Ile_{31}, and Met_{35} in red (A). ^{15}N-edited NOESY-HSQC spectrum of peptide **2d** showing key intermolecular NOEs to either Hα or *N*-Me (B) and NH protons (C). The spectrum was recorded at 11.0 mM in 9:1 H_2O/D_2O at 800 MHz and 298 K.

Species **B** exhibits six intermolecular **B**-**B** NOE contacts that are consistent with the intermolecular contacts at the interior vertices of the triangular trimers that comprise the peptide **2** crystallographic hexamer. Table **1** summarizes these six intermolecular contacts centered around the strong NOE between Lys_{16} Hα and Phe_{20} Hα shown in Figure **10A**. We excluded the possibility of the observed **B**-**B** NOEs arising from an antiparallel β-sheet dimer, in which Lys_{16} and Phe_{20} form a hydrogen-bonded pair, because the *N*-methyl group on Cha_{19} would disrupt hydrogen bonding at the dimer interface.

Table 1. Key intermolecular contacts observed for the peptide **2** oligomer.[a,b]

Interface			
A to **A**	**B** to **B**	**A** to **B (1)**[b]	**A** to **B (2)**[b]
Lys_{16} Hα to Leu_{34} Hα (m)[a]	Lys_{16} Hα to Phe_{20} Hα (s)[a]	Cha_{19} *N*-Me to Ile_{31} NH (m)[a]	Ile_{31} NH to Ile_{32} Hα (m)[a]
Lys_{16} Hα to Met_{35} NH (m)[a]	Lys_{16} Hα to Ala_{21} NH (m)[a]	Cha_{19} *N*-Me to Ile_{32} Hα (w)[a]	Ile_{31} NH to Gly_{33} NH (m)[a]
Leu_{17} NH to Gly_{33} NH (s)[a]	Leu_{17} NH to Cha_{19} *N*-Me (m)[a]	Phe_{20} Hα to Ala_{30} Hα (s)[a]	Ala_{30} Hα to Ile_{32} Hα (s)[a]
Leu_{17} NH to Leu_{34} Hα (w)[a]	Leu_{17} NH to Phe_{20} Hα (s)[a]	Phe_{20} Hα to Ile_{31} NH (m)[a]	Ala_{30} Hα to Gly_{33} NH (w)[a]
Leu_{17} NH to Met_{35} NH (w)[a]	Leu_{17} NH to Phe_{20} *Ar* (m)[a]	Phe_{20} *Ar* to Ile_{31} NH (m)[a]	
Val_{18} Hα to Ile_{32} Hα (m)[a]	Leu_{17} NH to Ala_{21} NH (m)[a]	Ala_{21} NH to Ala_{30} Hα (w)[a]	
Val_{18} Hα to Gly_{33} NH (m)[a]		Ala_{21} NH to Ile_{31} NH (m)[a]	
Cha_{19} *N*-Me to Ile_{31} NH (w)[a]			
Cha_{19} *N*-Me to Ile_{32} Hα (m)[a]			

[a]Letters in parentheses indicates the strength of the NOE as strong (s), medium (m), or weak (w).
[b]Number in parentheses indicates the two **A**-**B** interfaces.

Species **A** and **B** exhibit eleven intermolecular **A**-**B** NOE contacts that reveal how species **A** interfaces with the species **B** triangular trimer. These NOEs reflect two distinct interfaces between the **A** and **B** species. Seven of the NOEs involve a locus of contacts centered around the strong NOE between Ala_{30} Hα (species **B**) and Phe_{20} Hα (species **A**). Four of the NOEs reflect a locus of contacts centered around the strong NOE between Ile_{32} Hα (species **B**) and Ala_{30} Hα (species **A**). The observed pattern of **A**-**B** intermolecular contacts indicates that one molecule of species **A** forms intermolecular contacts with two adjacent molecules of species **B** as shown in Figure **10B**. The 1:1 integration between species **A** and **B** in conjunction with the two observed **A**-**B** interfaces suggest that species **A** assembles into a cylindrin-like trimer.

Species **A** exhibits a network of nine intermolecular NOEs consistent with the expected **A**-**A** intermolecular contacts within the cylindrin-like trimer (Table **1**). In the cylindrin, the KLVFFAE β-strand of each molecule forms an antiparallel interface with the AIIGLMV β-strand of the adjacent molecule. The nine intermolecular NOEs involving outer facing NH, Hα, and *N*-methyl protons of these two strands are consistent with orientation of the strands shown in Figure **10B**. Especially notable is a strong NOE between Leu_{17} NH and Gly_{33} NH, which is consistent with the contact between Leu_{17} and Gly_{33} shown in Figure **10C**. Collectively, these contacts between the KLVFFAE and AIIGLMV strands are consistent with the cylindrin-like trimer structure and are distinct from those that would be expected from a triangular trimer, such as that observed in the crystallographic hexamer.

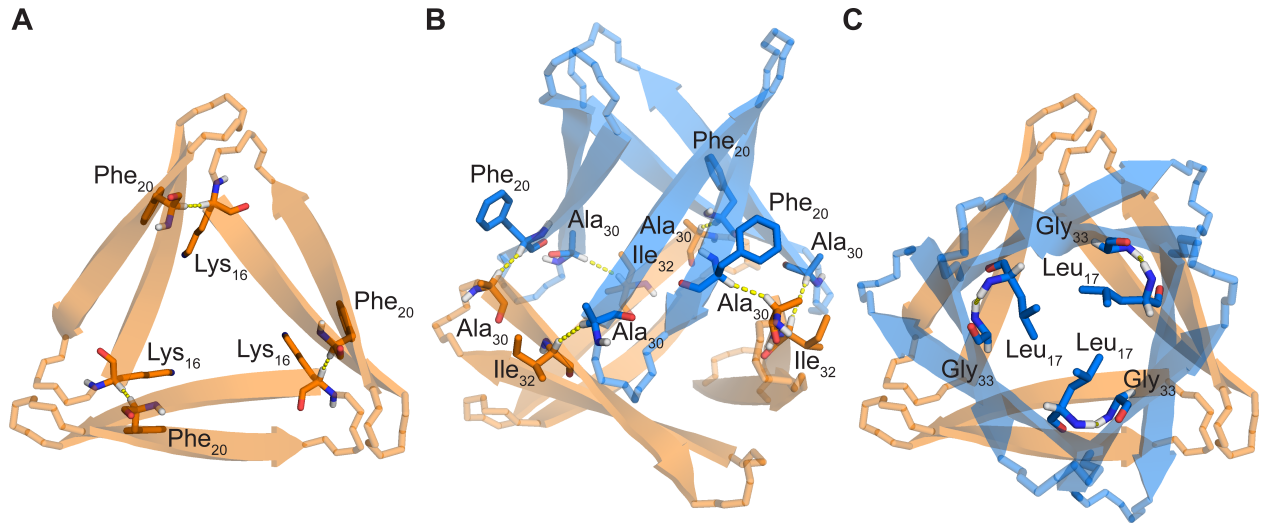

Figure 10. NMR-based molecular model of the asymmetric hexamer formed by peptide **2**. Species **A** is shown in blue and species **B** is shown in orange. (A) Top view of triangular trimer subunit formed by species **B** illustrating contacts between Lys_{16} and Phe_{20} within species **B**. (B) Side view of the hexamer illustrating contacts between Phe_{20} of species **A** and Ala_{30} of species **B** and between Ala_{30} of species **A** and Ile_{32} of species **B**. (C) Top view of the hexamer illustrating contacts between Leu_{17} and Gly_{33} within species **A**. The subunit formed by species **A** (blue) constitutes a cylindrin-like trimer.

ARTICLE

DOSY NMR suggests two asymmetric hexamers further assemble to form a dodecamer

We used DOSY NMR to further assess the oligomerization state of the asymmetric hexamer and found — to our surprise — that peptide **2** assembles into a well-defined oligomer that is larger than a hexamer (Figure **S14**). At 1.0 mM, the DOSY spectrum of peptide **2** shows one track associated with the diffusion coefficient of the monomer (1.98 x 10^{-10} m^2/s). At 6.0 mM, the DOSY spectrum shows multiple tracks corresponding to slow exchange on the NMR timescale between monomer and oligomer. At 11.0 mM, the DOSY spectrum shows one track associated with the diffusion coefficient of a well-defined oligomer (0.90 x 10^{-10} m^2/s).[30]

Our laboratory has previously characterized a variety of well-defined peptide tetramers using DOSY NMR and has consistently observed that the ratio of the diffusion coefficients of the oligomer and monomer reflects the oligomerization state in solution.[23,24,31–33] For compact structures, the diffusion coefficient scales as the negative cube root of the molecular weight. We have thus observed that the diffusion coefficients of tetramers are about 0.6 that of the monomers. For a hexamer, a ratio of 0.55 would be expected, and for a dodecamer, the ratio should be about 0.44. For peptide **2**, we observe a ratio of 0.46, which is too low to be consistent with a hexamer but is more consistent with that expected for a dodecamer. Other oligomers ranging from an octamer to a tetradecamer should have diffusion coefficients ratios ranging from 0.50 to 0.42, and thus cannot be rigorously distinguished by DOSY alone. The observed 1:1 integration ratio of NH and Hα proton resonances associated with species **A** and **B** in the ^{1}H NMR spectra rules out all odd-numbered oligomers. Additionally, our laboratory has observed multiple crystallographic assemblies of dodecamers formed by similar macrocyclic β-hairpin peptides.[22,34] Thus, the DOSY spectra, integration of both oligomer species, and crystallographic precedence collectively suggest that peptide **2** assembles into a dodecamer composed of two hexamers, rather than a single hexamer.

The solution-phase asymmetric hexamer shown in Figure **10** has multiple exposed hydrophobic surfaces, which could promote further assembly through hydrophobic interactions. The hydrophobic contacts between a pair of hexamers must be sufficiently rapid on the NMR timescale to allow the three **A** molecules of each hexamer to remain chemically equivalent to each other and the three **B** molecules of each hexamer to remain chemically equivalent to each other. The observation of a single track in the DOSY spectrum of peptide **2** at 11.0 mM supports that the exchange between the two hexamers is rapid on the NMR timescale.

Molecular dynamics simulations on a pair of hexamers

To better understand the structure of the putative dodecamer suggested by the DOSY NMR studies, we performed a series of MD simulations on pairs of hexamers using Amber22 with the ff19SB force field. The initial coordinates of the hexamers were generated from the constrained NMR-based molecular model. The MD simulations were performed without constraints within the hexamers for 500 ns in an NVT ensemble using a periodic box of explicit water. The MD simulations suggest that the asymmetric hexamers are stable and retain the same overall topology shown in Figure **10**. The asymmetric hexamers observed in the MD simulations are looser than the constrained NMR-based molecular model by about 3 Å backbone RMSD, reflecting the release of the constraints in the MD simulations (Figure **S15**). Intermolecular distances observed during MD simulations associated with key intermolecular NOEs are largely consistent with the NMR-based molecular model of the asymmetric hexamer (Figure **S16**).

The MD simulations reveal that the interactions between two asymmetric hexamers are dynamic. In three of the MD simulations the two hexamers remain in contact as a loose dodecamer, while in the other two MD simulations the loose dodecamer either comes apart to give two asymmetric hexamers or only stays as a dodecamer with imposed distance constraints (Figure **S17**). This dynamic behavior between two asymmetric hexamers is consistent with absence of specific NOE contacts associated with the dodecamer and variety of contacts between the hexamer subunits. (Figure **11**). The five MD simulations are further described in the Materials and Methods section of the Supporting Information.

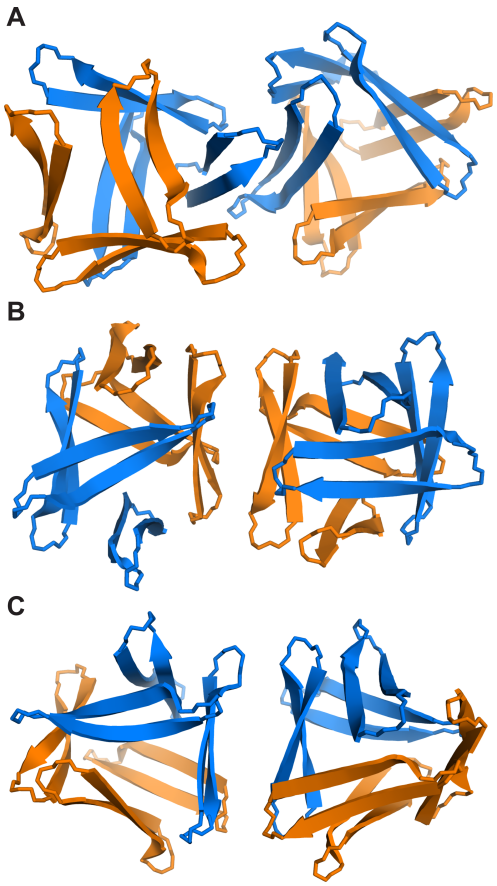

Figure 11. Three representative dodecamer configurations observed in different MD simulations. Species **A** is shown in blue and species **B** is shown in orange.

Effect of varying *N*-methylation on assembly in aqueous solution

To better understand which hydrogen bonds are crucial for the assembly of the asymmetric hexamer, we prepared homologues **3a–c** in which the position of *N*-methylation varies from that of peptide **2** (Table **2**). We started by shifting the position of *N*-methylation from Cha_{19} to Gly_{33} on peptide **3a**.[34] ^{1}H NMR spectroscopy indicates that peptide **3a** does not assemble to form well-defined oligomers at concentration up to 8.0 mM. The absence of assembly of peptide **3a** suggests that hydrogen bonding at Gly_{33} is important for the assembly of the asymmetric hexamer.

Table 2. Summary of peptide **2** analogues and their assembly in aqueous solution.

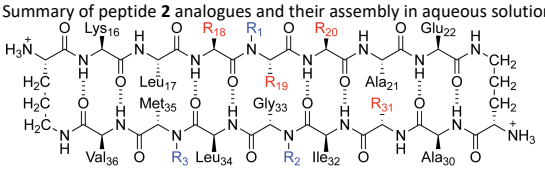

Peptide	R_1	R_2	R_3	R_{18}	R_{19}	R_{20}	R_{31}	Well-defined oligomer?
2	Me	H	H	Val	Cha	Phe	Ile	Yes
3a	H	Me	H	Val	Cha	Phe	Ile	No
3b	Me	Me	H	Val	Cha	Phe	Ile	No
3c	Me	H	Me	Val	Cha	Phe	Ile	Yes
4a	Me	H	H	Val	Cha	Phe	Chg	No
4b	Me	H	H	Val	Cha	Tyr	Ile	Yes
5	Me	H	H	Thr	Phe	Tyr	Ile	No

We prepared doubly methylated homologue **3b**, with methyl groups at Cha_{19} and Gly_{33}, to further probe the role of intermolecular hydrogen bonding between Leu_{17} and Gly_{33} within the cylindrin-like trimer formed by species **A**. Although peptide **3b** shows some propensity to oligomerize in the DOSY spectrum, we do not observe the formation of two discrete species in the ^{1}H NMR spectrum. The absence of two species suggests that intermolecular hydrogen bonds involving the Gly_{33} NH are critical to the formation of species **A** and **B**.

We also prepared doubly methylated homologue **3c**, with methyl groups at Cha_{19} and Met_{35}. The amide NH group of Met_{35} does not participate in hydrogen bonding in model of the asymmetric hexamer. We thus anticipated that *N*-methylation at Met_{35} should be tolerated. In solution, peptide **3c** assembles into a well-defined oligomer analogous to that of peptide **2**. The ^{1}H NMR spectrum of peptide **3c** at 1.0 mM is similar to that of peptide **2** at 1.0 mM, showing one set of resonances associated with monomer. The ^{1}H NMR spectrum of peptide **3c** at 11.0 mM is similar to that of peptide **2** at 11.0 mM, showing two sets of resonances associated with an oligomer.

Effect of hydrophilic and hydrophobic mutations on assembly in aqueous solution

To further probe the structures of the hexamer subunits of the dodecamer, we prepared homologues of peptide **2**, **4a** and **4b**, in which the amphiphilicity is augmented. Peptide **4a** increases the hydrophobicity of peptide **2** by mutating the interior residue Ile_{31} to cyclohexylglycine (Chg). The DOSY spectra show that peptide **4a** self-associates at lower peptide concentrations than peptide **2**. At 1.0 mM, the ^{1}H NMR spectrum is sharp and is similar to that of peptide **2**. At 6.0 mM, the ^{1}H NMR spectrum is broad, without distinct peaks for individual α-protons. The greater propensity of peptide **4a** to self-associate and the absence of a well-defined oligomer suggest that the steric bulk provided by both Cha_{19} and Chg_{31} is too great to permit the formation of a well-packed hydrophobic core of the hexamer subunit.

In peptide **4b**, we decreased the hydrophobicity of the exterior residue Phe_{20} by mutation to Tyr, with the hypothesis that the increased hydrophilicity would diminish uncontrolled aggregation and promote oligomerization. In solution, the propensity of peptide **4b** to form well-defined oligomers is comparable to that of peptide **2**. We also prepared peptide **5**, a homologue of peptide **1** with Phe_{20}-to-Tyr and Val_{18}-to-Thr mutations to explore whether increasing the hydrophilicity of exterior residues can promote oligomerization. Like peptide **1**, peptide **5** shows little propensity to oligomerize at concentrations up to 8.0 mM. Collectively, peptides **4b** and **5** demonstrate that hydrophilic mutations on exterior surfaces are tolerated but do not promote oligomer formation.

Conclusions

Aβ exhibits a remarkable propensity for supramolecular assembly. In the case of full-length Aβ, this assembly typically takes the form of aggregation into fibrils consisting of parallel β-sheets or oligomers with unknown structure. Fragments from the central and *C*-terminal regions of Aβ also have a propensity to aggregate. Macrocyclization and *N*-methylation permit these fragments to be tamed and crystallized into a well-defined oligomer. Strategic Phe-to-Cha mutation promotes assembly of a discrete well-defined oligomer, an asymmetric hexamer that differs in structure from that of the symmetric crystallographic hexamer.

Previously, our laboratory has only observed well-defined oligomer assembly by solution-phase NMR spectroscopy in a related class of macrocyclic β-hairpin peptides that contain Hao, a tripeptide mimic designed to template β-sheet formation. The planar character of Hao template biases the formation of sandwich tetramers in aqueous solution. Peptide **2** provides a more native-like model of Aβ β-hairpins in aqueous solution by reincorporating more of the native Aβ sequence. Solution-phase NMR spectroscopy shows that peptide **2** is the first *N*-methylated macrocyclic β-hairpin peptide to assemble to form a well-defined oligomer that can be characterized by solution-phase NMR spectroscopy. When compared to the Hao-containing peptides, peptide **2** adopts a much more twisted β-hairpin conformation, suggesting that the extent of hairpin twisting may influence the resulting oligomer that forms.

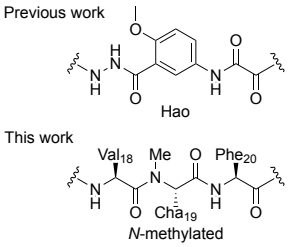

In aqueous solution, peptide **2** assembles into an asymmetric hexamer composed of a cylindrin-like trimer and a triangular trimer. Selective isotope incorporation (^{2}H and ^{15}N) proved essential both in enumerating the number of distinct species and identifying key intermolecular contacts, which were used to construct a molecular model of the asymmetric hexamer. DOSY NMR and MD simulations illustrate how the asymmetric hexamer can further assemble to form a loosely packed dodecamer composed of two hexamers. The presence of two distinct subunits and further supramolecular

assembly is reminiscent of the oligomer observed by Carulla and coworkers in their tetramer and octamer model of $A\beta_{1-42}$.[17,35]

The supramolecular assembly of Aβ oligomers into soluble oligomers continues to be of fundamental interest in understanding the molecular basis of Alzheimer's disease, yet the observation of soluble Aβ oligomers by solution-phase NMR spectroscopy has largely eluded researchers thus far. The solution-phase NMR studies of peptide **2** and its analogues contribute to the understanding of how amyloidogenic fragments from the central and *C*-terminal regions of Aβ can assemble to form well-defined oligomers in aqueous solution. The observation that peptide **2** forms a well-defined oligomer but peptide **1** does not suggests that these macrocyclic β-hairpin peptides teeter on the border of assembling into well-defined oligomers in aqueous solution. Studies on peptide **2** analogues demonstrate how solution-phase assembly depends on a delicate balance of intermolecular hydrogen bonding, hydrophobic interactions, and steric considerations. The characterization of well-defined oligomers of Aβ at atomic resolution continues to be an important and formidable challenge. We envision that *N*-methylation and hydrophobic Phe-to-Cha mutations may also be also useful in stabilizing other soluble Aβ oligomers and facilitating their observation by solution-phase NMR spectroscopy.

Author contributions

J.Z., A.G.K., and J.S.N. conceived the project, designed the experiments, and analysed the results; J.Z., X.L., and S.M.R. synthesized and characterized the peptides. J.Z. and A.G.K acquired the X-ray diffraction data. J.Z. collected the circular dichroism and SDS-PAGE data. J.Z performed the NMR experiments with support from X.L., and S. M. R. Z. L and V. P. performed theoretical investigations. J.Z. and J.S.N wrote and edited the paper.

Conflicts of interest

The authors declare no conflicts of interest.

Data availability

The data supporting this article have been included in the ESI† which includes: procedures for the synthesis and purification of peptide **1**–**5**; X-ray diffraction data collection, processing, and refinement of peptide **2**; silver-stained SDS-PAGE and circular dichroism spectroscopy; Fmoc-protection of ^{15}N-labeled amino acids; molecular modeling of the asymmetric hexamer; PyMOL model of the asymmetric hexamer, MD simulations on a pair of hexamers; solution NMR spectroscopy, HPLC, and MALDI-TOF characterization of peptides **1**–**5**. Crystallographic data for peptide **2** has been deposited under the PDB number 9EEC and can be obtained from https://www.rcsb.org/structure/unreleased/9EEC.

Acknowledgements

We thank Professor Nicholas L. Truex for providing some isotopically labeled Fmoc-protected amino acids. We thank Benjamin Katz and Dr. Felix Grun at the University of California Irvine Mass Spectrometry Facility for assistance with MALDI-TOF and Dr. Dmitry Fishman at the University of California Irvine Laser Spectroscopy Laboratory Laboratories for assistance with the circular dichroism measurements. The authors thank the NMR facility directors Dr. Suv Sengupta, Dr. John E. Kelly, and Dr. Phil R. Dennison for assistance with NMR experiments. We thank Joe Ziller at the X-ray Crystallographic Facility for assistance with crystallography. We thank the Advanced Light Source for allowing the acquisition of X-ray diffraction data. Beamline 5.0.2 of the Advanced Light Source, a DOE Office of Science User Facility under Contract No. DE-AC02-05CH11231, is supported in part by the ALS-ENABLE program funded by the National Institutes of Health, National Institute of General Medical Sciences, grant P30 GM124169-01. The authors thank the National Institute on Aging (Grant AG072587) and UCI ChemSURF NSF REU (CHE-1950126) programs for funding.

Notes and references

(1) Benilova, I.; Karran, E.; De Strooper, B. The Toxic Aβ Oligomer and Alzheimer's Disease: An Emperor in Need of Clothes. *Nat. Neurosci.* **2012**, *15* (3), 349–357. https://doi.org/10.1038/nn.3028.

(2) Cline, E. N.; Bicca, M. A.; Viola, K. L.; Klein, W. L. The Amyloid-β Oligomer Hypothesis: Beginning of the Third Decade. *J. Alzheimers Dis. 64* (Suppl 1), S567–S610. https://doi.org/10.3233/JAD-179941.

(3) Shankar, G. M.; Li, S.; Mehta, T. H.; Garcia-Munoz, A.; Shepardson, N. E.; Smith, I.; Brett, F. M.; Farrell, M. A.; Rowan, M. J.; Lemere, C. A.; Regan, C. M.; Walsh, D. M.; Sabatini, B. L.; Selkoe, D. J. Amyloid-β Protein Dimers Isolated Directly from Alzheimer's Brains Impair Synaptic Plasticity and Memory. *Nat. Med.* **2008**, *14* (8), 837–842. https://doi.org/10.1038/nm1782.

(4) Gremer, L.; Schölzel, D.; Schenk, C.; Reinartz, E.; Labahn, J.; Ravelli, R. B. G.; Tusche, M.; Lopez-Iglesias, C.; Hoyer, W.; Heise, H.; Willbold, D.; Schröder, G. F. Fibril Structure of Amyloid-β(1–42) by Cryo–Electron Microscopy. *Science* **2017**, *358* (6359), 116–119. https://doi.org/10.1126/science.aao2825.

(5) Kollmer, M.; Close, W.; Funk, L.; Rasmussen, J.; Bsoul, A.; Schierhorn, A.; Schmidt, M.; Sigurdson, C. J.; Jucker, M.; Fändrich, M. Cryo-EM Structure and Polymorphism of Aβ Amyloid Fibrils Purified from Alzheimer's Brain Tissue. *Nat. Commun.* **2019**, *10* (1), 4760. https://doi.org/10.1038/s41467-019-12683-8.

(6) Ghosh, U.; Thurber, K. R.; Yau, W.-M.; Tycko, R. Molecular Structure of a Prevalent Amyloid-β Fibril Polymorph from Alzheimer's Disease Brain Tissue. *Proc. Natl. Acad. Sci.* **2021**, *118* (4), e2023089118. https://doi.org/10.1073/pnas.2023089118.

(7) Yang, Y.; Arseni, D.; Zhang, W.; Huang, M.; Lövestam, S.; Schweighauser, M.; Kotecha, A.; Murzin, A. G.; Peak-Chew, S. Y.; Macdonald, J.; Lavenir, I.; Garringer, H. J.; Gelpi, E.; Newell, K. L.; Kovacs, G. G.; Vidal, R.; Ghetti, B.; Ryskeldi-Falcon, B.; Scheres, S. H. W.; Goedert, M. Cryo-EM Structures of Amyloid-β 42 Filaments from Human Brains. *Science* **2022**, *375* (6577), 167–172. https://doi.org/10.1126/science.abm7285.

(8) Frieg, B.; Han, M.; Giller, K.; Dienemann, C.; Riedel, D.; Becker, S.; Andreas, L. B.; Griesinger, C.; Schröder, G. F. Cryo-EM Structures of Lipidic Fibrils of Amyloid-β (1-40). *Nat. Commun.* **2024**, *15* (1), 1297. https://doi.org/10.1038/s41467-023-43822-x.

(9) Tycko, R. Solid State NMR Studies of Amyloid Fibril Structure. *Annu. Rev. Phys. Chem.* **2011**, *62*, 279–299. https://doi.org/10.1146/annurev-physchem-032210-103539.

(10) Durell, S. R.; Guy, H. R.; Arispe, N.; Rojas, E.; Pollard, H. B. Theoretical Models of the Ion Channel Structure of Amyloid Beta-Protein. *Biophys. J.* **1994**, *67* (6), 2137–2145. https://doi.org/10.1016/S0006-3495(94)80717-9.

(11) George, A. R.; Howlett, D. R. Computationally Derived Structural Models of the β-Amyloid Found in Alzheimer's Disease Plaques and the Interaction with Possible Aggregation Inhibitors. *Biopolymers* **1999**, *50* (7), 733–741. https://doi.org/10.1002/(SICI)1097-0282(199912)50:7<733::AID-BIP6>3.0.CO;2-7.

(12) Li, L.; Darden, T. A.; Bartolotti, L.; Kominos, D.; Pedersen, L. G. An Atomic Model for the Pleated β-Sheet Structure of Aβ Amyloid Protofilaments. *Biophys. J.* **1999**, *76* (6), 2871–2878. https://doi.org/10.1016/S0006-3495(99)77442-4.

(13) Hoyer, W.; Grönwall, C.; Jonsson, A.; Ståhl, S.; Härd, T. Stabilization of a β-Hairpin in Monomeric Alzheimer's Amyloid-β Peptide Inhibits Amyloid Formation. *Proc. Natl. Acad. Sci.* **2008**, *105* (13), 5099–5104. https://doi.org/10.1073/pnas.0711731105.

(14) Sandberg, A.; Luheshi, L. M.; Söllvander, S.; Pereira de Barros, T.; Macao, B.; Knowles, T. P. J.; Biverstål, H.; Lendel, C.; Ekholm-Petterson, F.; Dubnovitsky, A.; Lannfelt, L.; Dobson, C. M.; Härd, T. Stabilization of Neurotoxic Alzheimer Amyloid-β Oligomers by Protein Engineering. *Proc. Natl. Acad. Sci.* **2010**, *107* (35), 15595–15600. https://doi.org/10.1073/pnas.1001740107.

(15) Yu, L.; Edalji, R.; Harlan, J. E.; Holzman, T. F.; Lopez, A. P.; Labkovsky, B.; Hillen, H.; Barghorn, S.; Ebert, U.; Richardson, P. L.; Miesbauer, L.; Solomon, L.; Bartley, D.; Walter, K.; Johnson, R. W.; Hajduk, P. J.; Olejniczak, E. T. Structural Characterization of a Soluble Amyloid β-Peptide Oligomer. *Biochemistry* **2009**, *48* (9), 1870–1877. https://doi.org/10.1021/bi802046n.

(16) Itoh, S. G.; Yagi-Utsumi, M.; Kato, K.; Okumura, H. Key Residue for Aggregation of Amyloid-β Peptides. *ACS Chem. Neurosci.* **2022**, *13* (22), 3139–3151. https://doi.org/10.1021/acschemneuro.2c00358.

(17) Ciudad, S.; Puig, E.; Botzanowski, T.; Meigooni, M.; Arango, A. S.; Do, J.; Mayzel, M.; Bayoumi, M.; Chaignepain, S.; Maglia, G.; Cianferani, S.; Orekhov, V.; Tajkhorshid, E.; Bardiaux, B.; Carulla, N. Aβ(1-42) Tetramer and Octamer Structures Reveal Edge Conductivity Pores as a Mechanism for Membrane Damage. *Nat. Commun.* **2020**, *11* (1), 3014. https://doi.org/10.1038/s41467-020-16566-1.

(18) Kreutzer, A. G.; Spencer, R. K.; McKnelly, K. J.; Yoo, S.; Hamza, I. L.; Salveson, P. J.; Nowick, J. S. A Hexamer of a Peptide Derived from Aβ16–36. *Biochemistry* **2017**, *56* (45), 6061–6071. https://doi.org/10.1021/acs.biochem.7b00831.

(19) Kreutzer, A. G.; Hamza, I. L.; Spencer, R. K.; Nowick, J. S. X-Ray Crystallographic Structures of a Trimer, Dodecamer, and Annular Pore Formed by an $A\beta_{17–36}$ β-Hairpin. *J. Am. Chem. Soc.* **2016**, *138* (13), 4634–4642. https://doi.org/10.1021/jacs.6b01332.

(20) Nowick, J. S.; Brower, J. O. A New Turn Structure for the Formation of β-Hairpins in Peptides. *J. Am. Chem. Soc.* **2003**, *125* (4), 876–877. https://doi.org/10.1021/ja028938a.

(21) McKnelly, K. J.; Kreutzer, A. G.; Howitz, W. J.; Haduong, K.; Yoo, S.; Hart, C.; Nowick, J. S. Effects of Familial Alzheimer's Disease Mutations on the Assembly of a β-Hairpin Peptide Derived from Aβ16–36. *Biochemistry* **2022**, *61* (6), 446–454. https://doi.org/10.1021/acs.biochem.1c00664.

(22) Kreutzer, A. G.; Yoo, S.; Spencer, R. K.; Nowick, J. S. Stabilization, Assembly, and Toxicity of Trimers Derived from Aβ. *J. Am. Chem. Soc.* **2017**, *139* (2), 966–975. https://doi.org/10.1021/jacs.6b11748.

(23) Truex, N. L.; Wang, Y.; Nowick, J. S. Assembly of Peptides Derived from β-Sheet Regions of β-Amyloid. *J. Am. Chem. Soc.* **2016**, *138* (42), 13882–13890. https://doi.org/10.1021/jacs.6b06000.

(24) Pham, J. D.; Demeler, B.; Nowick, J. S. Polymorphism of Oligomers of a Peptide from β-Amyloid. *J. Am. Chem. Soc.* **2014**, *136* (14), 5432–5442. https://doi.org/10.1021/ja500996d.

(25) Senguen, F. T.; Lee, N. R.; Gu, X.; Ryan, D. M.; Doran, T. M.; Anderson, E. A.; Nilsson, B. L. Probing Aromatic, Hydrophobic, and Steric Effects on the Self-Assembly of an Amyloid-β Fragment Peptide. *Mol. Biosyst.* **2011**, *7* (2), 486–496. https://doi.org/10.1039/C0MB00080A.

(26) Haerianardakani, S.; Kreutzer, A. G.; Salveson, P. J.; Samdin, T. D.; Guaglianone, G. E.; Nowick, J. S. Phenylalanine Mutation to Cyclohexylalanine Facilitates Triangular Trimer Formation by β-Hairpins Derived from Aβ. *J. Am. Chem. Soc.* **2020**, *142* (49), 20708–20716. https://doi.org/10.1021/jacs.0c09281.

(27) We diluted an 11 mM solution of peptide **2** to 1 mM and observed that the sample re-equilibrated to the monomer on the order of hours. This experiment indicated that the equilibrium between monomer and oligomer is reversible and that the rate of exchange occurs slowly on the NMR timescale.

(28) Wishart, D. S.; Sykes, B. D. [12] Chemical Shifts as a Tool for Structure Determination. In *Methods in Enzymology*; Nuclear Magnetic Resonance, Part C; Academic Press, 1994; Vol. 239, pp 363–392. https://doi.org/10.1016/S0076-6879(94)39014-2.

(29) Laganowsky, A.; Liu, C.; Sawaya, M. R.; Whitelegge, J. P.; Park, J.; Zhao, M.; Pensalfini, A.; Soriaga, A. B.; Landau, M.; Teng, P. K.; Cascio, D.; Glabe, C.; Eisenberg, D. Atomic View of a Toxic Amyloid Small Oligomer. *Science* **2012**, *335* (6073), 1228–1231. https://doi.org/10.1126/science.1213151.

(30) Peptide **2** is not fully soluble at 16.0 mM. However, the nominal 16.0 mM DOSY spectrum gave a nearly identical diffusion coefficient (0.90×10^{-10} m^2/s), which suggests the soluble oligomer is well-defined.

(31) Li, X.; Rios, S. E.; Nowick, J. S. Enantiomeric β-Sheet Peptides from Aβ Form Homochiral Pleated β-Sheets Rather than Heterochiral Rippled β-Sheets. *Chem. Sci.* **2022**, *13* (26), 7739–7746. https://doi.org/10.1039/D2SC02080G.

(32) Khakshoor, O.; Demeler, B.; Nowick, J. S. Macrocyclic β-Sheet Peptides That Mimic Protein Quaternary Structure through Intermolecular β-Sheet Interactions. *J. Am. Chem. Soc.* **2007**, *129* (17), 5558–5569. https://doi.org/10.1021/ja068511u.

(33) Pham, J. D.; Spencer, R. K.; Chen, K. H.; Nowick, J. S. A Fibril-Like Assembly of Oligomers of a Peptide Derived from β-Amyloid. *J. Am. Chem. Soc.* **2014**, *136* (36), 12682–12690. https://doi.org/10.1021/ja505713y.

(34) Salveson, P. J.; Spencer, R. K.; Kreutzer, A. G.; Nowick, J. S. X-Ray Crystallographic Structure of a Compact Dodecamer from a Peptide Derived from Aβ16-36. *Org. Lett.* **2017**, *19* (13), 3462–3465. https://doi.org/10.1021/acs.orglett.7b01445.

(35) The Carulla tetramer and octamer model may differ from the asymmetric hexamer model because of the different β-hairpin registrations. The offset in hairpin registration by one residue alters the pattern of hydrogen bonding, pairing of amino acid side chains, and the resulting oligomer that forms.